Interhelical Ion Pairing in Coiled Coils: Solution Structure of a Heterodimeric Leucine Zipper and Determination of pK_a Values of Glu Side Chains[†,‡]

Daniel N. Marti,* Ilian Jelesarov, and Hans Rudolf Bosshard

Institute of Biochemistry, University of Zürich, CH-8057 Zürich, Switzerland

Received May 31, 2000; Revised Manuscript Received August 8, 2000

ABSTRACT: Residues of opposite charge often populate heptad positions *g* (heptad *i* on chain 1) and *e′* (heptad *i* + 1 on chain 2) in dimeric coiled coils and may stabilize the dimer by formation of interchain ion pairs. To investigate the contribution to stability of such electrostatic interactions we have designed a disulfide-linked heterodimeric zipper (AB zipper) consisting of the acidic chain Ac-E−VAQLEKE−VAQAEAE−NYQLEQE−VAQLEHE−CG-NH_2 and the basic chain Ac-E−VQALKKR−VQALKAR−NYAAKQK−VQALRHK−CG-NH_2 in which all *e* and *g* positions are occupied by either E or K/R to form a maximum of seven interhelical salt bridges. Temperature-induced denaturation experiments monitored by circular dichroism reveal a stable coiled coil conformation below 50 °C and in the pH range 1.2−8.0. Stability is highest at pH ∼ 4.0 [ΔG_U (37 °C) = 5.18 ± 0.51 kcal mol^{-1}]. The solution structure of the AB zipper at pH 5.65 has been elucidated on the basis of homonuclear ^{1}H NMR data collected at 800 MHz [heavy atom rmsd's for the ensemble of 50 calculated structures are 0.47 ± 0.13 Å (backbone) and 0.95 ± 0.16 Å (all)]. Both chains of the AB zipper are almost entirely in α-helical conformation and form a superhelix with a left-handed twist. Overhauser connectivities reveal close contacts between *g* position residues (heptad *i* on chain 1) and residues *d*/*f* (heptad *i* on chain 1), residues *a*/*d* (heptad *i* + 1 on chain 1), and residue *a′* (heptad *i* + 1 on chain 2). Residues in position *e* (heptad *i* on chain 1) are in contact with residues *a*/*b*/*d*/*f* (heptad *i* on chain 1) and residue *d′* (heptad *i* on chain 2). These connectivities hint at a relatively defined alignment of the side chains across the helix interface. Partial H-bond formation between the functional groups of residues *g* and *e′*(+1) is observed in the calculated structures. NMR pH titration experiments disclose pK_a values for Glu δ-carboxylate groups: 4.14 ± 0.02 (E^1), 4.82 ± 0.07 (E^6), 4.52 ± 0.01 (E^8), 4.37 ± 0.03 (E^{13}), 4.11 ± 0.02 (E^{15}), 4.41 ± 0.07 (E^{20}), 4.82 ± 0.03 (E^{22}), 4.65 ± 0.04 (E^{27}), 4.63 ± 0.03 (E^{29}), 4.22 ± 0.02 ($E^{1'}$). By comparison with pK_a of Glu in unfolded peptides (∼4.3 ± 0.1), our pK_a data suggest marginal or even unfavorable contribution of charged Glu to the stability of the AB zipper. The electrostatic energy gained from interhelical ion pairs is likely to be surpassed by hydrophobic energy terms upon protonation of Glu, due to increased hydrophobicity of uncharged Glu and, thus, better packing against apolar residues at the chain interface.

Two-stranded α-helical coiled coils, proposed by Crick in 1953 (*1*), have been identified in a wide variety of proteins such as transcription factors (*2*) and fibrous proteins (*3*). In basic transcription factors (bZIP),[1] the coiled coil forming domain (zipper domain) comprises 30−40 residues and is located at the C-terminal end of the protein next to a basic DNA binding segment. Dimerization and binding to DNA of the bZIP occur simultaneously and are largely mediated by the formation of a stable coiled coil structure (*4*−*6*). The strength of DNA···bZIP interaction therefore strongly depends on the capability of the zipper domain to establish a stable dimeric coiled coil.

The superhelix formation of the zipper domain has its origin in several repeats of a seven-residue sequence motif $(abcdefg)_n$: positions *a* and *d* are frequently occupied by hydrophobic residues such as Val and Leu, whereas the remaining positions comprise preferably polar or charged residues. A number of X-ray crystallographic and NMR studies aimed at the elucidation of coiled coil structures including those of bZIP transcription factors (*5*, *7*−*12*), tropomyosin (*13*, *14*), and trimeric matrilin-1 (*15*). In two-stranded parallel coiled coils, the side chains of residues

[†] This research was supported by Grants BBW 97.0592 and SNF 31.55308.98.

[‡] The coordinates have been submitted in the Brookhaven Protein Databank (file name 1FMH).

* To whom correspondence should be addressed. Phone: +41 1 635 5545, fax: +41 1 635 6805, e-mail: dmarti@access.unizh.ch.

[1] Abbreviations: 2D, two-dimensional; AB zipper, heterodimeric disulfide-linked coiled coil consisting of peptides Ac-EVAQLEKEVAQAEAENYQLEQEVAQLEHECG-NH_2 and Ac-EVQALKKRVQALKARNYAAKQKVQALRHKCG-NH_2; AcGluOMe, N^{α}-acetyl-glutamic acid methyl ester; bZIP, basic region leucine zipper family of transcription factors; CD, circular dichroism; CDIH, dihedral angle restraint; COSY, 2D chemical shift correlated spectroscopy; DQF, double quantum filtered; DTT, dithiothreitol; EM, energy minimization; Fmoc, 9-fluorenylmethoxycarbonyl; HBTU, *O*-benzotriazol-1-yl-*N*,*N*,*N*′,*N*′-tetramethyluronium hexafluorophosphate; K_a, equilibrium proton association constant; MD, molecular dynamics; NOE, nuclear Overhauser effect; NOESY, 2D NOE correlated spectroscopy; pH*, glass electrode pH reading, uncorrected for deuterium isotope effect; RT, room temperature; θ, ellipticity; TOCSY, 2D total correlation spectroscopy; rmsd, root-mean square deviation; sc, side chain; τ_m, mixing time; TPPI, time proportional phase increment; TSP, sodium 3-(trimethylsilyl)-[2,2,3,3-D_4]propionate; vdW, van der Waals.

10.1021/bi001242e CCC: $19.00
Published on Web 09/29/2000

located at the interface of the juxtaposed helices pack according to a "knobs-into-holes" model (*1*). The kinetics of folding and the coupled thermodynamic stability of the dimeric zipper are highly dependent on the type of residues in positions *a*, *d*, *e*, and *g* shaping the interface of the coiled coil (*16*−*22*). In many bZIPs, one hydrophobic residue located in the *a* position of a central heptad is substituted by polar Asn interrupting the hydrophobic interface. It has been shown that Asn in such position is slightly destabilizing the coiled coil and preventing the formation of higher order polymers (*8*, *16*, *17*, *23*, *24*).

Although the driving force for the stabilization of the coiled coil structure is the hydrophobic packing of *a* and *d* as well as *e* and *g* position residues at the chain interface, the latter are also thought to play an important role in stabilizing/destabilizing the dimeric zipper by imposing attractive/repulsive interhelical electrostatic interactions. It has been well-established that ionic repulsion among *g* and *e*′(+1) residues[2] prevents the formation of stable dimers (*21*, *22*, *25*−*28*). While intrahelical ion pairs between residues spaced *i*, *i* + 3, and *i*, *i* + 4 might stabilize the coiled coil (*29*, *30*), the occurrence of interhelical *g*···*e*′(+1) salt bridges and their contribution to stability of coiled coils is under debate (*31*, *32*). Double mutant cycle studies on designed coiled coils suggest favorable electrostatic energy terms at neutral pH resulting from interhelical ion pairing between *g* and *e*′(+1) position residues (*33*), Glu···Arg being more stabilizing than Glu···Lys (*34*).

The contribution of an ionizable group to the free energy of folding (ΔG_F) is reflected in the difference in the pK_a value determined for the folded and unfolded protein (*32*, *35*). In the crystal structure of GCN4, two interchain salt bridges are apparent (*8*). However, relative to the unfolded protein, NMR pH titration experiments reveal very minor shifts of pK_a values, indicative of negligible contribution of the charged residues to stability (*36*). Continuum electrostatics calculations on the mono- and dimeric helices of the GCN4 crystal structure disclose unfavorable desolvation effects upon docking of the helices that largely exceed the electrostatic energy gained by interhelical ion pairs (*30*). Furthermore, determination of Glu pK_a values in matrilin-1 (*37*) and kinetic studies on oppositely charged dimeric zippers (*20*) suggest no or only minor favorable contributions of interhelical ion pairs to protein stability.

To gain more detailed insight into the complex interdependence between electrostatic and hydrophobic effects in coiled coils, we have begun a systematic study on the thermodynamics and kinetics of folding of a designed heterodimeric, disulfide-linked coiled coil called AB zipper. It is composed of an acidic and a basic peptide chain in which all *e*/*g* positions are occupied by either Glu or Lys/Arg, enabling the formation of seven interchain ion pairs (Figure 1). In this paper, we report the high-resolution solution structure of the AB zipper solved on the basis of ^{1}H NMR data recorded at 800 MHz. pK_a values of all 10 Glu residues in the zipper have been determined and are discussed with respect to structural data and the pH dependence of the coiled coil stability investigated by thermal unfolding. To our knowledge, this is the first study to report Glu pK_a values for each *e* and *g* heptad position in a dimeric coiled coil.

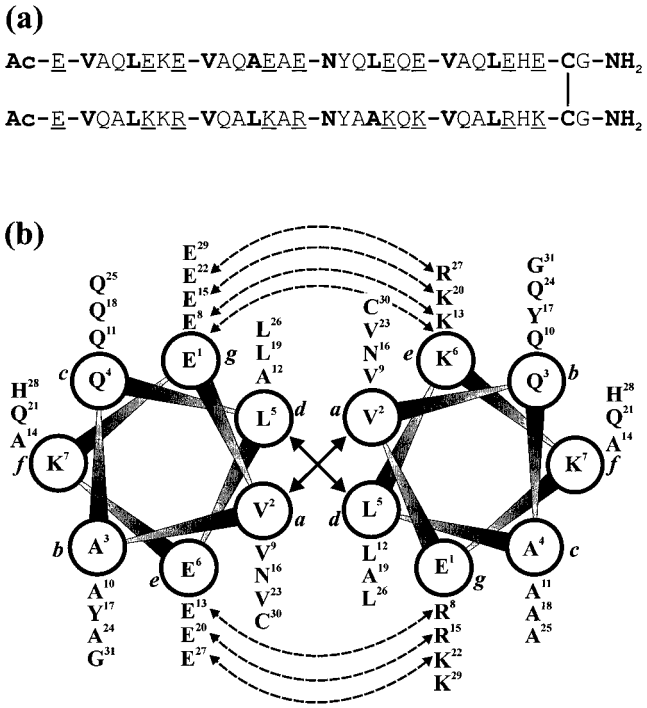

FIGURE 1: Primary sequence and helix wheel representation of the heterodimeric AB zipper. (a) The amino acid sequences of the disulfide-linked acidic (top) and basic (bottom) peptides are displayed. Heptad sequence motifs are separated by dashes, and the disulfide bond is indicated by a vertical line. Residues in *a* and *d* heptad positions are in boldface, and residues in *e* and *g* positions are underlined. (b) Helix wheel representation of the aligned acidic (left side) and basic (right side) helices. Heptad positions are denoted by lower case letters in italic. Interhelical hydrophobic interactions involving *a* and *d* positions residues and potential ion pairing between amino acids in positions *e* and *g* are highlighted by solid and dashed arrows, respectively.

EXPERIMENTAL PROCEDURES

Peptide Synthesis and Purification. Peptides A and B were synthesized on a Perkin-Elmer ABI 433 A solid-phase peptide synthesizer using the Rink amide methylbenzhydrylamine resin (*38*) from Novabiochem (Läufelfingen, Switzerland), the Fmoc protection strategy, and HBTU coupling. Removal of the N-terminal Fmoc group, N-terminal acetylation, deprotection of side chains, except for *S*-(*tert*-butylthio)Cys, and the release of the peptides from the resin as C-terminal amides were performed as described (*20*−*22*). Removal of the *tert*-butyl-thio protection group from Cys occurred by incubation in the presence of a 100-fold molar excess of DTT in water at 55 °C for 18 h. Final purification was achieved by size-exclusion chromatography on a Sephadex G-25 column and by HPLC (Hewlett-Packard 1100) using a C_{18} column (Machery-Nagel Nucleosil, 250 × 10 mm, 100 Å pore size, 5 μm particle size) and linear acetonitrile gradient from 24 to 48% (slope of 0.53% min^{-1}; flow rate of 1.2 mL min^{-1}). To obtain the disulfide-linked AB zipper, 10 mg of both peptides dissolved in 10 mL of 50 mM NH_4HCO_3, pH 8, were gently stirred for 48 h at RT while exposed to the air; the product was purified by HPLC as described above. Electrospray mass analysis on a Perkin-Elmer/Sciex API III+ spectrometer yielded the expected

[2] Positive and negative numbers in parentheses indicate up- and downstream shifts in heptads; dashes designate heptad positions in the adjacent helix.

masses of 3557 and 3576 Da for the acidic and basic chains, respectively, and 7131 Da for the disulfide-linked heterodimer.

CD Spectroscopy. Spectra were acquired on a Jasco J-715 spectropolarimeter at 20 °C in a buffer composed of boric, citric, and phosphoric acid, each at 7.5 mM. The pH was adjusted in the range of 1.2−8 by adding HCl or KOH, and the ionic strength was kept at 0.1 M by adding KCl. Spectra were recorded from 195 to 250 nm at 5 nm/min and 0.2-nm resolution and averaged over three scans. Temperature-induced reversible denaturation was monitored by following the change in θ at 222 nm. Data points were acquired at 20 s intervals with a bandwidth of 1 nm. The temperature was increased from 5 to 90 °C at 0.7 °C min^{-1}. The sample was allowed to equilibrate for 20 min before heating and the reversibility of the denaturation was probed by monitoring θ during cooling of the sample to the starting temperature.

Assuming a two-state unfolding reaction (*39*), the observed θ_{obs} is composed of

$$\theta_{obs}(T) = f_U(T)[\theta_U(0) + m_U T] + [1 - f_U(T)][\theta_F(0) + m_F T] \quad (1)$$

$\theta_U(0)$ and $\theta_F(0)$ are the θ values of the unfolded and folded protein, respectively, at the chosen reference temperature of 0 °C. m_U and m_F are the slopes of the linear temperature dependence of θ of the unfolded and folded protein, respectively, and $f_U(T)$ is the fraction of unfolded protein. $f_U(T)$ relates to the Gibbs free energy of unfolding $\Delta G_U(T)$:

$$f_U(T) = \exp[-\Delta G_U(T)/RT]/\{1 + \exp[-\Delta G_U(T)/RT]\} \quad (2)$$

$\Delta G_U(T)$ is expressed by the Gibbs−Helmholtz equation:

$$\Delta G_U(T) = \Delta H_U(T_m)[1 - T/T_m] + \Delta C_p\{T - T_m - T\ln[T/T_m]\} \quad (3)$$

T_m is the transition midpoint temperature, $\Delta H_U(T_m)$ is the apparent transition enthalpy of unfolding at T_m, and ΔC_p is the difference in the heat capacity between the folded and unfolded state. ΔC_p was calculated according to refs *22* and *40* using the NMR structures and a linear, extended model peptide as templates. The calculated ΔC_p was ∼0.5 kcal mol^{-1} K^{-1}. $\theta_U(0)$, m_U, $\theta_F(0)$, m_F, $\Delta H_U(T_m)$, and T_m were fitted to the experimental CD data applying a nonlinear least-squares fitting routine. T_m was verified by a minima search in the first derivative of eq 1.

NMR Data Acquisition and Processing. The AB zipper was dissolved in 555 μL of 90% H_2O/10% D_2O (99.996 atom % D, Cambridge Isotope Lab., Andover, MA) at a concentration of 2.12 mM, and the pH* was adjusted to 5.65 by the addition of NaOD or DOAc. Data were recorded at 37 °C in quadrature on Bruker Avance DRX-800 and DRX-600 spectrometers operating at 800 and 600 MHz, respectively, using 5-mm TXI triple resonance z-gradient probes. The DQF-COSY (*41*) experiment was acquired with 600 complex points along t_1 applying Sates-TPPI (*42*), and water suppression was achieved with low-power irradiation during the 1 s relaxation delay between scans. The TOCSY experiment was recorded with the MLEV-17 (*43*), DIPSI-2 (*44*), or clean CITY (*45*) sequence for isotropic mixing (τ_m of 35, 66, and 72 ms, respectively). The NOESY experiment was acquired with various τ_m set between 25 and 350 ms. For the latter two experiments, between 512 and 600 complex t_1 points were collected in TPPI or States mode. Water suppression was accomplished with gradients via the watergate (*46*) or 3-9-19 (*47*) pulse sequences. t_2 data were routinely acquired with 2 K complex points, and the carrier was positioned on the water frequency in both t_1 and t_2 using spectral widths of 8012.8 Hz (800 MHz) or 6009.6 Hz (600 MHz).

Raw data were processed with the program FELIX v.98 (Molecular Simulations Inc., San Diego, CA) on a Silicon Graphics Indy R4400 workstation. t_1 time domain data were zero filled to 2 K complex points. Resolution enhancement was achieved by applying straight (DQF-COSY) or 45°-shifted squared (TOCSY, NOESY) sine-bell window functions along both t_1 and t_2 (*48*). Correction of the baseline was accomplished with a model-free algorithm (*49*). The matrix size of processed spectra was kept at 2 K × 2 K points. For a high-resolution spectrum of the DQF-COSY experiment (4 K × 4 K points), Gaussian multiplication of the t_2 data was performed before Fourier transformation. ^{1}H chemical shifts are referred to the TSP resonance using *p*-dioxane as an internal standard (*50*).

pH Titration. The dependence of proton chemical shifts on the pH* was monitored by acquiring a total of 13 2D TOCSY experiments (70 ms of MLEV-17 mixing; 256 complex t_1 points) at pH* values in the range 1.5−7. The AB zipper was dissolved in 700 μL of 90% H_2O/10% D_2O at a concentration of 2.44 mM, and spectra were recorded at 37 °C on a Bruker DRX-500 spectrometer as described above. The pH* in the sample was adjusted by adding small amounts of HCl or NaOH from stock solutions, after transferring the sample to an Eppendorf tube and temperature equilibration for 10 min at 37 °C. Off NMR tube pH* readings at 37 °C were repeated after transferring the sample back to the NMR tube once and after the acquisition of the NMR data. All three readings were consistent within 0.03 pH units.

The pH* dependence of Glu H^{γ} and backbone H^N chemical shifts was analyzed according to refs *51* and *52*:

$$\delta(\mathrm{pH}) = \frac{\delta_a + \delta_b 10^{n(\mathrm{pH} - \mathrm{p}K_a)}}{1 + 10^{n(\mathrm{pH} - \mathrm{p}K_a)}} \quad (4)$$

δ_a and δ_b are the chemical shift plateaus of proton resonances at the acidic and basic pH limits, respectively, and n is the Hill coefficient. Nonlinear least-squares fitting to eq 4 was performed with δ_a, δ_b, and pK_a as free evolving parameters. n was either fixed at 1 or included as a free variable to probe for cooperativity.

Interproton Distances, Stereospecific Assignment, and Torsion Angle Restraints. A total of 2492 NOE connectivities were unambiguously assigned in the 2D NOESY spectra. Distances[3] were estimated from 1494 cross-peaks after measuring either volumes in the 150 ms NOESY experiment or the volume buildup in NOE experiments acquired with τ_m of 25, 50, 75, and 100 ms. A total of 578 restraints were intraresidue, 318 were sequential, 418 were medium-range ($1 < |i - j| < 5$) and 180 were long-range ($5 \leq |i - j|$), the

[3] Among these, 369 defined backbone−backbone, 780 backbone−side chain, and 345 side chain−side chain interactions.

latter connecting protons across the chain interface. Fixed interproton separation of vicinal H^{β} and amide protons were used for the calibration of distances according to the r^{-6} relationship between NOE cross-peak volumes and distances. Upper limits were calculated by adding 30% of the estimated distance as well as the appropriate pseudo atom distance correction (*53*). Lower limits were set to 1.8 Å.

H^N-H^{α} spin−spin coupling constants ($^3J_{HN\alpha}$) were derived from the high-resolution DQF-COSY spectrum by spectral simulation of the cross-section along t_2 of cross-peaks connecting H^N to H^{α}. $^3J_{HN\alpha} \leq 5.5$ Hz was identified for 52 residues for which torsion angles ϕ were assigned to lie within −30° to −90° (*54*, *55*). Stereospecific assignments of H^{β} were obtained for residues in *a* and *d* positions of the heptads on the basis of $^3J_{\alpha\beta}$ estimates from the DQF-COSY spectrum, and the H^N-H^{β} and H^{α}-H^{β} NOE intensities (τ_m of 150 ms). χ_1 torsion angles of Asn$^{16,16'}$ were restrained to 180 ± 30° and −60 ± 30°, respectively, consistent with $^3J_{\alpha\beta}$, and $H^N_{(i)}$-$H^{\beta}_{(i)}$, $H^N_{(i+1)}$-$H^{\beta}_{(i)}$ and $H^{\alpha}_{(i)}$-$H^{\beta}_{(i)}$ NOE data. Stereospecific assignments of the Val γ-methyl groups were based on $^3J_{\alpha\beta}$ and on $H^N_{(i)}$-$H^{\gamma}_{(i)}$, $H^N_{(i+1)}$-$H^{\gamma}_{(i)}$ and $H^N_{(i)}$-$H^{\beta}_{(i)}$ NOE intensities.

Structure Calculation. Computation of 50 structures was performed according to a distance geometry/simulated annealing protocol (*56*−*58*), using the program X-PLOR v.3.851 (*59*) and the "parallhdg5.0.pro" force field (*60*). After the embedding of backbone and β/γ carbon atoms into a metric matrix on the basis of experimental constraints, unknown atom coordinates were least-squares fitted to the embedded coordinates with ideal covalent geometry. Chirality and planarity were introduced during 4.5 ps of high temperature MD at 1500 K. In the succeeding three runs of simulated annealing (6 ps each), vdW interactions were gradually increased while cooling stepwise from 1500, 1000, and 600 K, respectively, to 100 K. Regularized structures were Powell energy minimized in 200 steps. In the penultimate MD run, the distance between the S^{γ} atoms of pairing Cys$^{30/30'}$ was constrained by a NOE. In the last MD run, the S^{γ}'s were covalently linked. Throughout the calculation, the NOE energy was modeled by a square-well function using the center averaging option for ambiguously assigned methylene and methyl protons. The vdW energy was represented by a repel function using a variable force constant.

To avoid artifacts due to the simple repulsive potential for the nonbonded energy term, an 8-Å shell of explicit TIP3P model water and an electrostatic energy term were introduced in the further refinement (*60*, *61*). MD simulations included heating to 500 K (1.25 ps), equilibration at 500 K (12.5 ps), and cooling to 100 K (5 ps). The energy of the final structures was Powell minimized in 200 steps. vdW and electrostatic energies were represented by switched and shifted functions, respectively, effective in the range from 6.5 to 8.5 Å. A soft-square function was used for modeling the NOE energy. The quality of the structures was assessed with the programs PROCHECK-NMR v.3.4.4 (*62*) and WHAT IF v.97 (*63*). Geometric properties were examined with the software MOLMOL v.2.6 (*64*) and with X-PLOR. The latter was also used for the computation of the solvent accessible surface using a solvent probe radius of 1.4 Å. Calculations were carried out on a Silicon Graphics Onyx2 workstation.

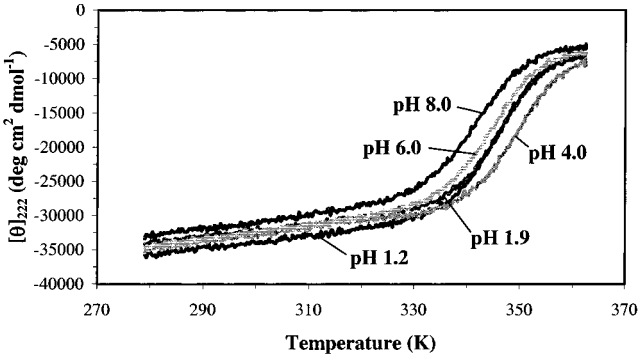

FIGURE 2: pH dependence of the thermal stability of the AB zipper. CD thermal unfolding curves recorded on 14 μM AB zipper at an ionic strength of 0.1 M and at pH values of 8.0, 6.0, 4.0, 1.9, and 1.2 are superimposed.

Table 1: Thermodynamic Parameters of Temperature-Induced Unfolding of the AB Zipper Determined by CD: pH Dependence of T_m, $\Delta H_U(T_m)$, and ΔG_U (310 K) at an Ionic Strength of 0.1 M

pH	T_m (K)[a]	$\Delta H_U(T_m)$ (kcal mol^{-1})[a]	ΔG_U (310 K) (kcal mol^{-1})[b]
1.2	345.5 ± 0.4	53.1 ± 2.1	4.52 ± 0.45
1.9	346.4 ± 0.3	53.1 ± 2.3	4.60 ± 0.47
4.0	349.4 ± 0.2	56.1 ± 3.3	5.18 ± 0.51
6.0	344.6 ± 0.4	49.5 ± 2.2	4.07 ± 0.42
8.0	341.6 ± 0.5	46.4 ± 1.6	3.54 ± 0.38

[a] Values were obtained by nonlinear least-squares fitting of the CD data to eq 1. [b] ΔG_U was calculated on the basis of the fitted T_m and $\Delta H_U(T_m)$ applying a ΔC_p of 0.5 kcal mol^{-1} K^{-1}. ΔC_p was estimated from the difference in solvent-exposed surface area of the folded and linear, extended protein (*40*). Errors were estimated assuming an error in ΔC_p of 0.5 kcal mol^{-1} K^{-1}.

RESULTS AND DISCUSSION

The sequence of the AB zipper and the location of the putative interhelical ionic bonds are shown in Figure 1. Net charges of the peptides at neutral pH are −8 (acidic chain) and +8 (basic chain). Localization of Val and Leu/Ala residues in positions *a* and *d*, respectively, and Asn in the *a*-position of the third heptad ensure parallel and in-register orientation of the chains in the dimer (*4*, *8*, *10*, *12*, *16*, *23*). Positions *b*, *c*, and *f* are occupied by α-helix stabilizing residues, and Tyr in position *b* of the third heptad enables the determination of the peptide concentration from near-UV absorption (*65*).

CD Spectroscopy. To investigate the pH dependence of the secondary structure content, CD spectra were recorded at pH values of 1.2, 1.9, 4.0, 6.0, and 8.0, respectively, at an ionic strength of 0.1 M. Minima at 208 and 222 nm were observed in all spectra, evidence for α-helical structure being preserved within the investigated pH range. [θ_{222}] varied from −34 410 deg cm^2 dmol^{-1} at pH 1.2 to −31 990 deg cm^2 dmol^{-1} at pH 8.0. These values are typical for proteins in almost fully α-helical conformation (*21*, *66*, *67*). The stability of the AB zipper was examined by temperature-induced denaturation experiments (Figure 2). Thermodynamic parameters calculated from thermal unfolding are given in Table 1. Two state folding/unfolding is supported by differential scanning calorimetry (data not shown). The AB zipper is most stable at pH ∼4.0. Stability decreases slightly at lower and higher pH values.

Resonance Assignment and Identification of Secondary Structure. Amino acid spin systems were identified on the

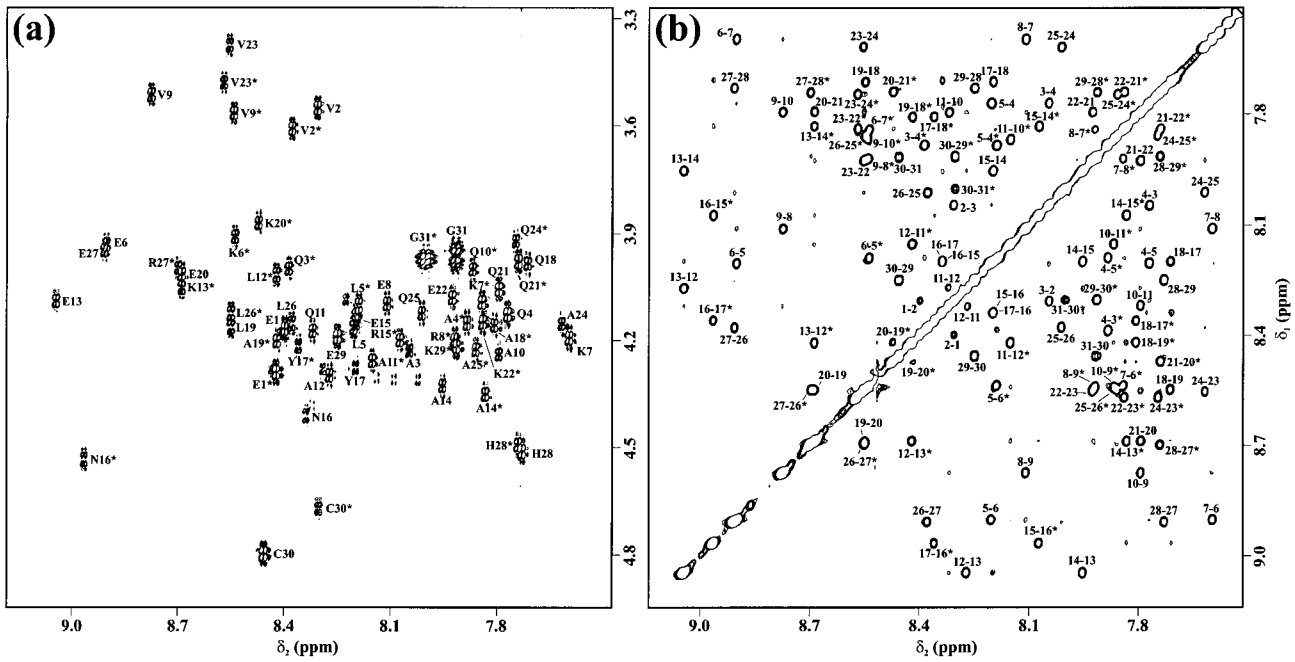

FIGURE 3: Spectral segments of the ^{1}H NMR DQF-COSY and 150 ms NOESY recorded on the AB zipper. (a) $H^N_{(i)}$-$H^\alpha_{(i)}$ cross-peaks in the "fingerprint" area of the DQF-COSY. Labels identify cross-peaks stemming from residues in the acidic and basic (marked by stars) chain of the zipper. (b) Labeled cross-peaks in the amide region of the NOESY spectrum represent connectivities between $H^N_{(i)}$ and $H^N_{(i+1)}$. Connected proton pairs are denoted by numbers (stars designate cross-peaks of the basic chain) using matrix convention (column proton-row proton). Cross-peaks between $H^N_{(i)}$ and $H^N_{(i+2,i+3)}$ appear only weak or are not visible at the selected contour level. Connectivities between $E^{1'}$-$V^{2'}$ and $V^{2'}$-$Q^{3'}$ are not observed due to H^N frequency overlap. Spectra were recorded on a 2.12 mM sample dissolved in 90% H_2O/10% D_2O at pH* 5.65 and 37 °C.

basis of 2D DQF-COSY and TOCSY experiments. The "fingerprint" area of the COSY spectrum is well-resolved comprising 62 cross-peaks connecting H^N to H^α (Figure 3, panel a). In contrast to what is observed for the homodimeric leucine zippers GCN4 (*7*) and c-Jun (*11*), resonances from residues located at identical positions in the two juxtaposed helices of the heterodimeric AB zipper differ in chemical shifts. Most of the residues display high-field shifted H^α resonances, by comparison to the random coil conformation (*68*): this is evidence for helical structure in the AB zipper. H^α resonances of most Ala and of residues located at the N- and C-terminal ends such as $Glu^{1,1'}$, $Cys^{30,30'}$, and $Gly^{31,31'}$ show moderate low-field shift changes. The sequential identification of the amino acids was obtained from the 2D NOESY spectra. Except for the N-terminal residues $Glu^{1'}$−$Gln^{3'}$, which disclose similar H^N chemical shifts, strong $H^N_{(i)}$-$H^N_{(i+1)}$ cross-peaks are observed between neighboring residues along both the acidic and the basic peptide chains (Figure 3, panel b, and Figure 4). Moreover, the presence of NOE cross-peaks of medium intensity connecting $H^{\alpha/\beta}_{(i)}$ to $H^N_{(i+1)}$ is further evidence for the integrity of the sequential residue assignment. In helical secondary structure, short distances (<5 Å) are observed between protons H^α-$H^N_{(i+2,i+3,i+4)}$, $H^N_{(i)}$-$H^N_{(i+2)}$, and $H^\alpha_{(i)}$-$H^\beta_{(i+3)}$ (*69*, *70*). A large number of NOE cross-peaks connecting the corresponding protons have been identified in the AB zipper (Figure 4). The pattern of connectivities among backbone and side chain protons strongly suggests the occurrence of α-helical structure within the entire acidic and basic peptide chains, which is further supported by $^3J_{HN\alpha}$ extracted from the DQF-COSY spectrum: 52 residues displayed $^3J_{HN\alpha} < 5.5$ Hz (Figure 4) suggesting backbone ϕ torsion angles of $\sim -60°$ typical for α-helical conformation. $^3J_{HN\alpha} < 5.5$ Hz is also compatible with positive ϕ values (*55*). Nevertheless, positive ϕ are energetically unfavorable (*69*, *71*) and have been rarely observed in protein structures. Resonance assignments of the AB zipper are provided as Supporting Information.

AB Zipper Structure. Initially, 50 structures were calculated in a vacuum based on the experimental NMR restraints (Figure 5, panel a) without applying an energy term for electrostatic interactions. The ensemble of 50 calculated structures converged: heavy atom rmsd of 0.78 ± 0.27 Å (backbone) and 1.24 ± 0.27 Å (all atoms) for the peptide segments Val^2−Glu^{29} and $Val^{2'}$−$Lys^{29'}$. Convergence was further improved by introducing an 8-Å shell of TIP3P model water molecules (*61*) and by applying a term for electrostatic interactions during the MD simulation in the last refinement step (*60*): heavy atom rmsd of 0.47 ± 0.13 Å (backbone) and 0.95 ± 0.16 Å (all atoms). Overall, the structures displayed a good covalent geometry and were in agreement with the experimental NMR restraints (Table 2). The quality of the backbone ϕ and ψ angle conformation was probed with the program PROCHECK-NMR: 97.1% of the ϕ/ψ angle pairs fell into the energetically most favored, 2.3% into the additional allowed, 0.3% into the generously allowed, and 0.3% into disallowed areas. A total of 25 structures were selected on the basis of their total energy, quality of the covalent geometry, and agreement with experimental restraints (Table 2).

Both the acidic and the basic peptide chains are almost entirely in α-helical conformation and wrap around each other in parallel orientation (Figure 6, panel a). Residues displaying backbone rmsd < 0.5 Å are found within the four central heptads, namely, residue segments Ala^3−Leu^{26} of the acidic and $Leu^{5'}$−$Leu^{26'}$ of the basic chain, while backbone atoms of residues located at the N- and C-terminal ends of

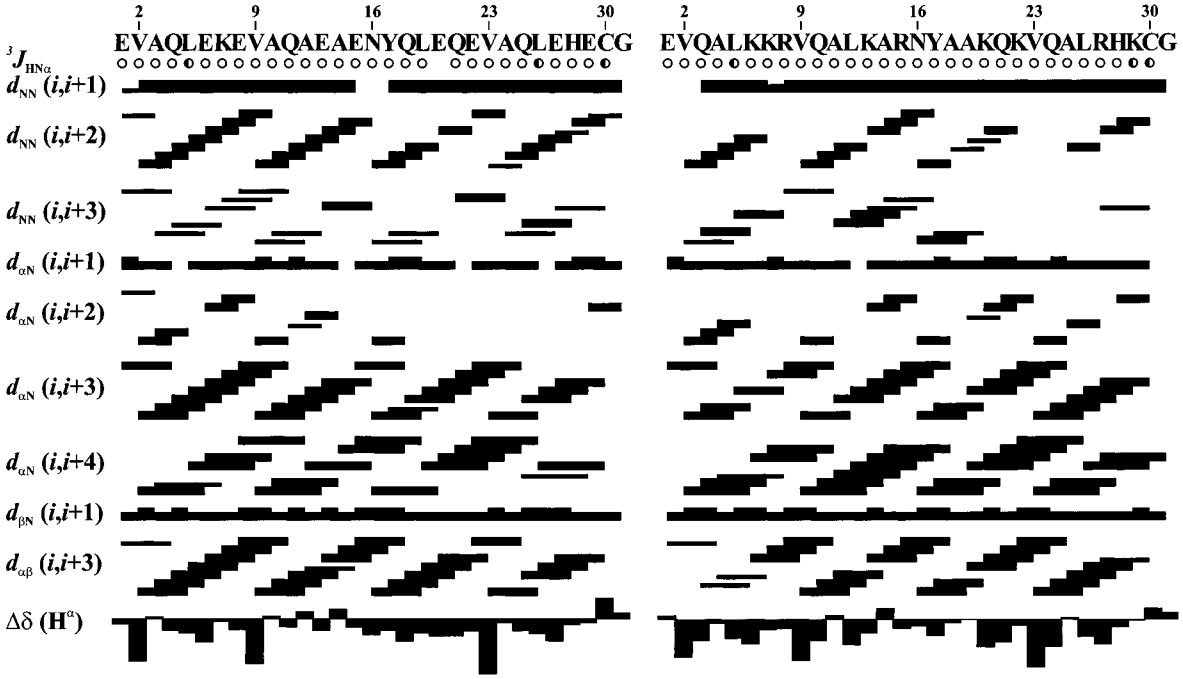

FIGURE 4: Summary of $^3J_{HN\alpha}$ couplings, backbone proton NOE connectivities, and H^α chemical shift changes. H^N-H^α couplings ($^3J_{HN\alpha}$) were measured in the DQF-COSY spectrum and are depicted by empty ($^3J_{HN\alpha} \leq 5.5$ Hz) and half-filled (5.5 Hz $\leq {}^3J_{HN\alpha} \leq 8$ Hz) circles. Intensities of NOE cross-peaks connecting $H^N_{(i)}$ to $H^N_{(i+1,i+2,i+3)}$, $H^\alpha_{(i)}$ to $H^N_{(i+1,\ i+2,i+3,i+4)}$, $H^\beta_{(i)}$ to $H^N_{(i+1)}$, and $H^\alpha_{(i)}$ to $H^\beta_{(i+3)}$ were determined in the 2D NOESY spectrum recorded with τ_m of 150 ms. The widths of the bars represent the relative intensities of the NOE cross-peaks. The extent of H^α chemical shift change $\Delta\delta(H^\alpha)$ relative to random coil H^α shift (*68*) is illustrated by bars. The primary sequence of the acidic (left side) and basic (right side) chain is shown. Experimental conditions were as described in the legend of Figure 3.

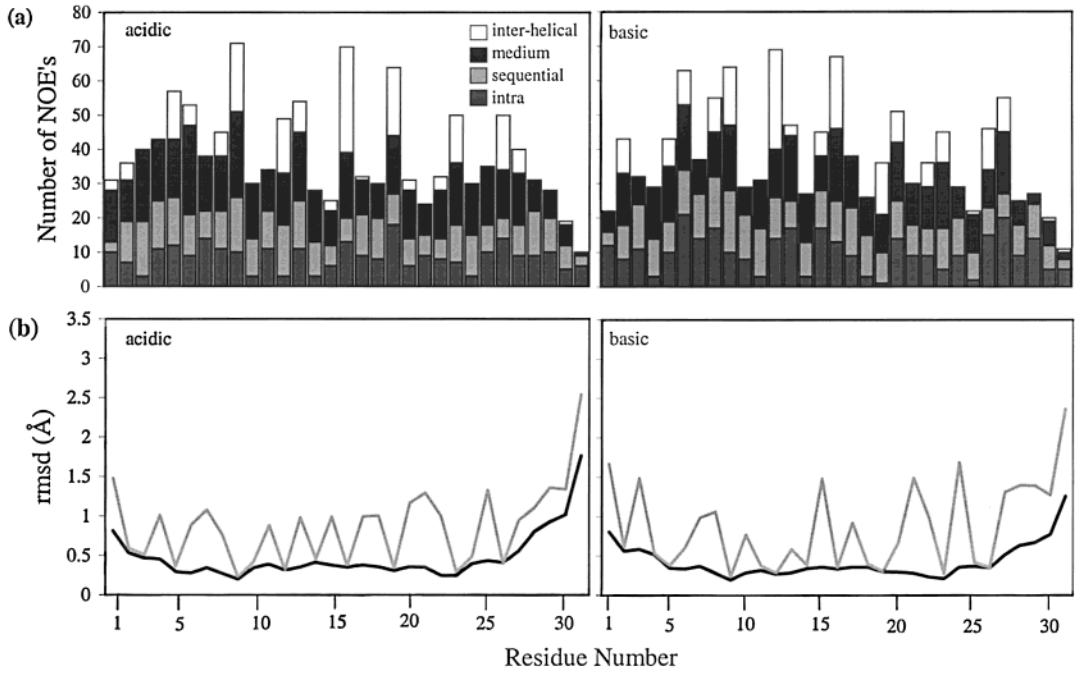

FIGURE 5: Comparison between the number of distance constraints per residue and the averaged heavy atom rmsd from the mean for the acidic and basic chain in the AB zipper. (a) The number of intraresidue, sequential, medium-range ($1 < |i\text{-}j| < 5$), and interhelical NOE constraints is represented by bars filled with different grades of shading. (b) The averaged rmsd to the mean of backbone heavy atoms N, C^α, and C′ (black) and of side chain heavy atoms (gray) is plotted versus the sequence number. Determination of rmsd values was performed on the set of 25 selected structures.

the dimer are relatively disordered (Figure 5, panel b). The superhelical twist of the single chains is left-handed as observed in other coiled coils (*8*, *10*, *12*, *14*). Overall, the AB zipper has a cylindrical shape with the approximate height of ~41 Å and width of ~18 Å. Best-fit alignment of the AB zippers' backbone heavy atoms of the four heptads with the corresponding atoms of the GCN4 crystal structure yields an rmsd of 0.85 ± 0.14 Å. Hence, the overall fold of the designed heterodimeric AB zipper determined by NMR very closely matches the fold of natural nondisulfide-linked GCN4 obtained by X-ray crystallographic methods (*8*). The C-terminal disulfide bond formed by *a* position residues

Table 2: Structural Statistics of the AB Zipper: Heavy Atom rmsd, rmsd of Geometric Terms, and Energy Summary

	ensemble of 50 structures	25 selected structures
rmsd from the mean of heavy atom coordinates[a]		
backbone (Å)	0.47 ± 0.13	0.38 ± 0.11
all (Å)	0.95 ± 0.16	0.81 ± 0.09
rmsd of experimental restraints[b]		
NOE all (Å)	0.031 ± 0.018	0.018 ± 0.003
intraresidue (Å)	0.022 ± 0.012	0.014 ± 0.007
sequential (Å)	0.029 ± 0.022	0.016 ± 0.004
medium ($1 < \|i - j\| < 5$) (Å)	0.038 ± 0.027	0.021 ± 0.003
long ($5 \leq \|i - j\|$) (Å)	0.027 ± 0.011	0.019 ± 0.002
CDIH (deg)	0.68 ± 0.95	0.10 ± 0.08
rmsd of geometric terms[c]		
bonds (Å)	0.005 ± 0.002	0.003 ± 0.0002
angles (deg)	0.59 ± 0.19	0.47 ± 0.03
impropers (deg)	0.56 ± 0.22	0.42 ± 0.03
averaged energies[d]		
NOE (kcal mol^{-1})	66.7 ± 74.8	14.8 ± 6.4
CDIH (kcal mol^{-1})	7.6 ± 12.7	0.1 ± 0.1
bonds (kcal mol^{-1})	29.5 ± 28.7	11.4 ± 1.6
angles (kcal mol^{-1})	117.2 ± 88.9	62.3 ± 7.0
impropers (kcal mol^{-1})	31.5 ± 28.9	13.7 ± 1.8
van der Waals (kcal mol^{-1})	−174.0 ± 59.7	−212.3 ± 9.4
electrostatic (kcal mol^{-1})	−2875.6 ± 53.4	−2881.4 ± 50.5

[a] Relative to the Val^{2}−Glu^{29} and Val$^{2'}$−Lys$^{29'}$ peptide segments of the mean structure, generated by averaging the coordinates of the selected ensemble after best-fit superimposition of backbone N, C$^{\alpha}$, and C′ atoms. [b] rmsd values for experimental distance and angle constraints represent the deviation from upper and lower limits applied in the structure calculation. [c] rmsd of geometric terms were determined by reference to the idealized covalent geometry as defined in the "parallhdg5.0.pro" force field (*60*). [d] Energies were calculated using the force field "parallhdg5.0.pro" and the OPLSX nonbonded parameter set (*72*). van der Waals and electrostatic energies were modeled by switched and shifted functions, respectively, using a dielectric constant of $\epsilon_0 = 1$. Force constants of 50 kcal mol^{-1} Å^{-2} and 200 kcal mol^{-1} rad^{-2} were applied for the calculation of NOE and CDIH energy terms.

Cys$^{30/30'}$ only marginally affects the integrity of the coiled coil structure. After best-fit superimposition of the GCN4 structure and the minimized average structure of the AB zipper, the averaged displacements of N, C$^{\alpha}$, and C′ atoms of *a* position residues of the four heptads amount to 0.57, 0.56, and 0.64 Å, respectively. For the corresponding atoms in Cys$^{30/30'}$, displacements of 0.64, 0.79, and 1.35 Å result. The relatively large displacement of C′ is a consequence of the lower structural definition of the C-terminal end of the zipper.

The curvature of the juxtaposed helices is due to the $CO_{(i)}\cdot\cdot\cdot HN_{(i+4)}$ H-bond lengths being dependent on the position of the N−H bond vector in the heptad. HN groups of residues located at or close to the chain interface such as those of *a*, *d*, and *e* position residues are involved in shorter H-bonds than those of residues in positions *b*, *c*, *f*, or *g* pointing toward the solvent (*8*, *12*, *73*). The periodicity of the H-bond length is reflected in the H^{N} chemical shifts. Less pronounced high field shifts are expected for H^{N} resonances participating in the short H-bonds of the α-helix. The H-bond lengths in the AB zipper were predicted using an empirical function (*74*). In agreement with previously determined structures, short H-bond lengths[4] result for residues in positions *a*, *d*, and *e* while significantly longer H-bond lengths are obtained for residues in positions *b*, *c*, *f*, and *g* (Figure 7, panel a).

Alignment of Residues in Positions a and d. X-ray and NMR studies on coiled coils (*5*, *8*, *10*, *12*, *14*) have shown that side chains of interface residues pack according to Crick's "knobs-into-holes" model (*1*). In this model, residue *a* of one peptide chain is surrounded by residues *a*′, *d*′, *d*′(−1), and *g*′(−1) forming a "hole" in the adjacent helix. Likewise, residue in position *d* of one helix forms a "knob" which is in close contact with residues *a*′, *d*′, *e*′, and *a*′(+1) of the adjacent chain. A total of 177 of the 180 NMR-derived interchain distances[5] represent such interactions across the dimer interface.

The spatial orientation of the C$^{\alpha}$−C$^{\beta}$ bond is determined by the backbone conformation of the protein. Because of the α-helical conformation of the two chains in the AB zipper and their relative orientation in the dimer, the C$^{\alpha}$−C$^{\beta}$ bond of residues in positions *a* packs in parallel orientation relative to the vector defined by C$^{\alpha}$ atoms of residues in positions *a*′ and *g*′(−1) on the juxtaposed strand. Residues in position *d* pack in such a way that the C$^{\alpha}$−C$^{\beta}$ bond is aligned perpendicularly relative to the vector formed by C$^{\alpha}$ atoms of residues in positions *d*′ and *e*′. Such alignment of residues at the chain interface is in line with the "knobs-into-holes" packing model (*17*) and is typically found in coiled coils (*8*, *10*, *12*).

The averaged χ_1 angle for all six Val residues in the set of 25 selected structures is 173.4 ± 7.6°, which matches the energetically preferred χ_1 rotamer of 180°. Corresponding Val's in the crystal structure of GCN4 and in c-Jun have an averaged χ_1 of 177° (*8*, *10*). The six Leu residues of the AB zipper in position *d* exhibit $\chi_1 = -64.0 \pm 8.7°$ and $\chi_2 = 173.2 \pm 9.3°$, in good agreement with the preferred rotamers of Leu (χ_1 and χ_2 of −60° and 180°, respectively) and with Leu rotamers in other coiled coils (*8*, *10*, *12*).

[4] These are 1.93 ± 0.06 Å (1.89 ± 0.02 Å), 1.93 ± 0.04 Å (1.92 ± 0.02 Å), and 1.90 ± 0.02 Å (1.94 ± 0.03 Å) for residues in *a*, *d*, and *e* positions, and 2.11 ± 0.07 Å (2.09 ± 0.09 Å), 2.09 ± 0.07 Å (2.09 ± 0.05 Å), 2.20 ± 0.08 Å (2.18 ± 0.03 Å), and 2.12 ± 0.04 Å (2.14 ± 0.03 Å) for residues in *b*, *c*, *f*, and *g* positions of the acidic (basic) chain.

[5] Twenty-four NOEs are observed between *a* and *a*′, 14 between *d* and *d*′, 17 between *a* and *d*′, 23 between *a* and *d*′(−1), 42 between *a* and *g*′(−1), and 57 between *d* and *e*′ position residues. One pertains to *d*−c′ and two pertain to *b*−*d*′(−1) interactions.

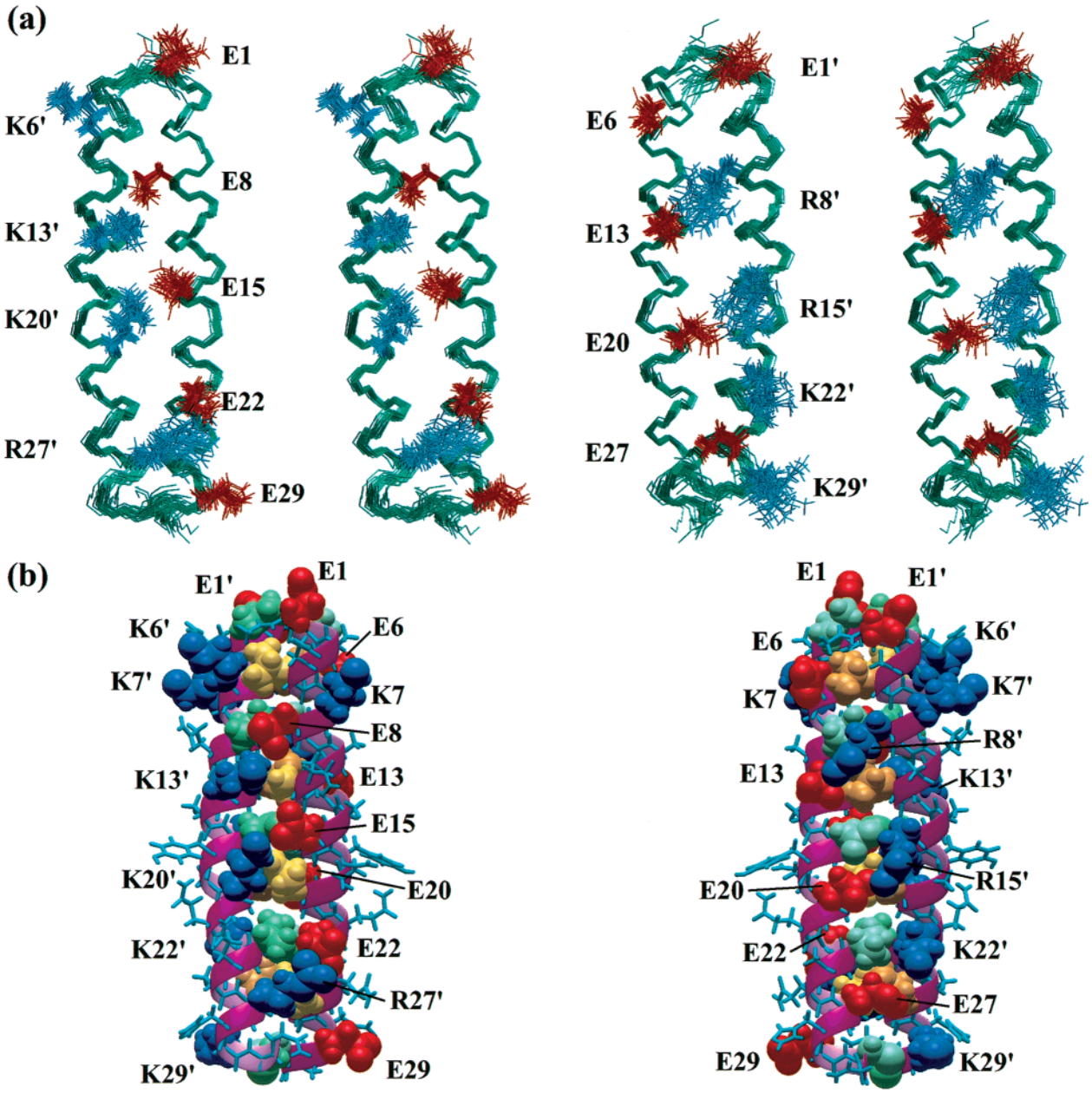

FIGURE 6: Alignment of charged residues in the ensemble of 25 selected AB zipper structures. (a) Stereoviews of the spatial orientation of *e* and *g* position residues in the acidic and basic helix are shown. Side chain bonds of acidic and basic residues are displayed in red and blue, respectively, and backbone bonds are outlined in green. (b) Representation of the minimized average structure obtained from the set of 25 selected structures. Atoms of charged residues and of amino acids in positions *a* and *d* are drawn in vdW space filling mode. Acidic and basic residues are colored in red and blue, respectively, and a color code of green and yellow is applied for residues in positions *a* and *d*. Side chain and backbone bonds are displayed in stick and ribbon representation, respectively. Front and back views of the zipper are shown. The figures were created with the program MOLMOL v.2.6 (*64*).

In the AB zipper, proton frequencies of Asn$^{16,16'}$ are distinguishable, indicating substantial structural asymmetry in the peptide segment. DQF-COSY spectra reveal strong $^3J_{\alpha\beta}$ couplings involving Asn^{16} H$^{\beta 3}$ of the acidic and Asn$^{16'}$ H$^{\beta 2}$ of the basic chain, while $^3J_{\alpha\beta}$ couplings to the corresponding vicinal H$^{\beta}$ are only weak. NOE cross-peak intensity ratios of the connectivities between H^N-H$^{\beta 2}$ and H^N-H$^{\beta 3}$ amount to 1.12 for Asn^{16} and 1.66 for Asn$^{16'}$, while those between H$^N_{(i+1)}$-H$^{\beta 2}_{(i)}$ and H$^N_{(i+1)}$-H$^{\beta 3}_{(i)}$ yield intensity ratio values of 0.55 (Asn^{16}) and 1.12 (Asn$^{16'}$), respectively. Such pattern of scalar and dipolar couplings suggest that Asn$^{16,16'}$ of the acidic and basic chain adopt χ_1 rotamer conformations of 180° and −60°, respectively. By comparison, the crystal structure of GCN4 exhibits χ_1 of −68.2° and −174.7° (*8*). Interestingly, NMR studies on the GCN4 (*7*) and c-Jun homodimers (*10*, *16*) reveal only one set of resonances for the conserved Asn consistent either with a symmetrical packing of Asn in solution or with a fast exchange between asymmetrical conformations that cannot be resolved on the NMR time scale at RT (*16*, *75*).

Alignment of Charged Residues in Positions e and g. Charged residues in the heptad positions *e* and *g* can modulate the stability of the coiled coils as well as the specificity of dimerization (*27*, *28*, *34*). Thus, folding of a dimeric zipper containing exclusively Glu in each *e* and *g* position on both chains is prevented above pH 6 due to interhelical charge repulsion (*21*, 22, *27*). Moreover, the preference of c-Jun-Fos and the c-Myc-Max for heterodimer

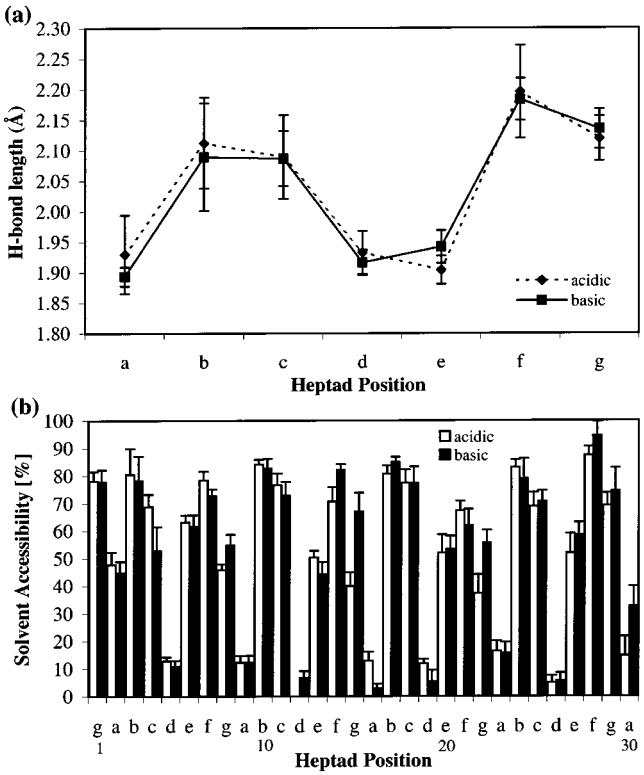

FIGURE 7: Predicted H-bond length between $CO_{(i)}$ and $NH_{(i+4)}$ groups and relative solvent accessibilities of side chains in the AB zipper. (a) The H-bond length was calculated on the basis of the H^N chemical shift according to an empirical function (*74*) and averaged for each heptad position in the acidic (solid line) and basic (dashed line) helix, respectively. H-bonds within the four central heptad pairs in the zipper were considered for the averaging. (b) The relative solvent accessibilities of side chains in the acidic (white bars) and basic (black bars) helices are plotted versus the heptad position. Solvent accessibilities determined for side chains in a linear peptide using three Gly as spacer between different residue types served as the 100% reference. Data represent the averaged accessibilities derived for the ensemble of 25 selected structures.

formation results from attractive (heterodimer) and repulsive (homodimer) electrostatic interactions of ionic residues in *g* and *e′*(+1) positions (*25*, *76*). In the designed AB zipper, all *e* and *g* positions are occupied by Glu in the acidic, and by Lys or Arg in the basic chain. All together, seven attractive and one repulsive interhelical electrostatic interactions are possible: $E^1(g0)-K^{6'}(e'1)$, $E^{1'}(g'0)-E^6(e1)$, $E^8(g1)-K^{13'}(e'2)$, $R^{8'}(g'1)-E^{13}(e2)$, $E^{15}(g2)-K^{20'}(e'3)$, $R^{15'}(g'2)-E^{20}(e3)$, $E^{22}(g3)-R^{27'}(e'4)$, $K^{22'}(g'3)-E^{27}(e4)$. Between 10 and 44 NOE-derived interresidue distance constraints per amino acid were applied in the structure calculations to determine the spatial alignment of the charged residues (Figure 5, panel a). In general, the rmsd values of the residues correlate with the number of unambiguously assigned NOE constraints. The conformations of Glu, Lys, and Arg side chains in the set of 25 selected structures are depicted in Figure 6, panel a. Inspection of the side chain NOEs of the charged residues reveals the preferred partners for interresidue interactions (Table 3). Residues in *g* position of heptad *i* are prone to be close to residues in positions *d* and *f* of the same heptad as well as with residues *a* and *d* of heptad $i + 1$. Furthermore, a significant number of interactions with residue *a′* in heptad $i + 1$ of the juxtaposed helix is observed. In contrast, *e* position residues interact mainly with residues

Table 3: Number of NOE Distance Constraints Derived for Side Chain Protons of *e* and *g* Position Residues

	same chain									juxta chain	
position	*a*	*b*	*c*	*d*	*f*	*a* (+1)	*b* (+1)	*c* (+1)	*d* (+1)	*a* (+1)	*d*
*g*0 (E^1)						1	5	4		2	
*g*1 (E^8)				5		4				6	
*g*2 (E^{15})				1	1	2			3	2	
*g*3 (E^{22})				2		1		1	1	3	
*g*4 (E^{29})			1	2		2					
*g*0′ ($E^{1'}$)						1	1	2			
*g*1′ ($R^{8'}$)				1	1	6			3	8	
*g*2′ ($R^{15'}$)				1	1	4				7	
*g*3′ ($K^{22'}$)			1	1		2			4	7	
*g*4′ ($K^{29'}$)				1		2					
*e*1 (E^6)	2	5		1	3						2
e2 (E^{13})	5	4		3	4						4
*e*3 (E^{20})	1	2			1						1
*e*4 (E^{27})	2	2			4						3
*e*1′ ($K^{6'}$)	4	2			4						6
e2′ ($K^{13'}$)	3	2			2						2
*e*3′ ($K^{20'}$)		3			3						5
*e*4′ ($R^{27'}$)	3	4			1						6

in positions *a*, *b*, *d*, and *f* of the same heptad, while no distance constraints to residues of the consecutive heptad have been found. In addition, all *e* position residues show a large number of interactions to residue *d′* of heptad *i* located on the opposite helix. Such pattern of NOE-derived distances imposes a defined alignment of the residues' side chains across the chain interface (Figure 6). Indeed, residues in *g* and *e′*(+1) positions point against each other in such a way that partial H-bonding occurs in the calculated structures. An exception is $Lys^{6'}$, for which no H-bond interaction to Glu^1 is observed due to the low structural definition of the N-terminal residue. Likewise, no H-bond partners are detected for the side chains of Glu^{29} and $Lys^{29'}$ located close to the C-terminal ends. Comparison of the averaged structure of the ensemble calculated in a vacuum, without applying an electrostatic function, with the averaged structure of the ensemble derived in the presence of a water shell reveals a very similar orientation of the charged side chains. Hence, the alignment of the charged residues results from the applied distance restraints and is not just a consequence of switching on the electrostatic term in the last refinement step. Inspection of NOESY spectra recorded with long τ_m reveals no unambiguous NOE cross-peaks connecting side chain protons of the suggested ion pairs. The lack of NOEs between the charged residues, although the average distance between Glu H^γ and Lys/Arg H^ϵ is 4.82 ± 0.51 Å in the structures, hints at a large mobility of the charged side chains leading to cancellation of the dipolar couplings. Since no distance restrains between charged *g* and *e′*(+1) position residues were applied in the structure calculation, the spatial alignment of those residues is exclusively imposed by intrahelical restraints as well as restraints to *a′*(+1) or *d′* position residues of the juxtaposed chain (Table 3). The latter interactions are consistent with the "knobs-into-holes" packing of helices (*1*) in which close contacts between $a(+1)-g'$ and $d-e'$ residues are formed. The interactions with hydrophobic *a* and *d* position residues of the helix-interface imply that *e* and *g* position residues contribute to the hydrophobic core of the coiled coil (Figure 8). The alignment of the acidic and basic residues across the hydrophobic chain interface is apparently a consequence of both ionic interactions among side chain

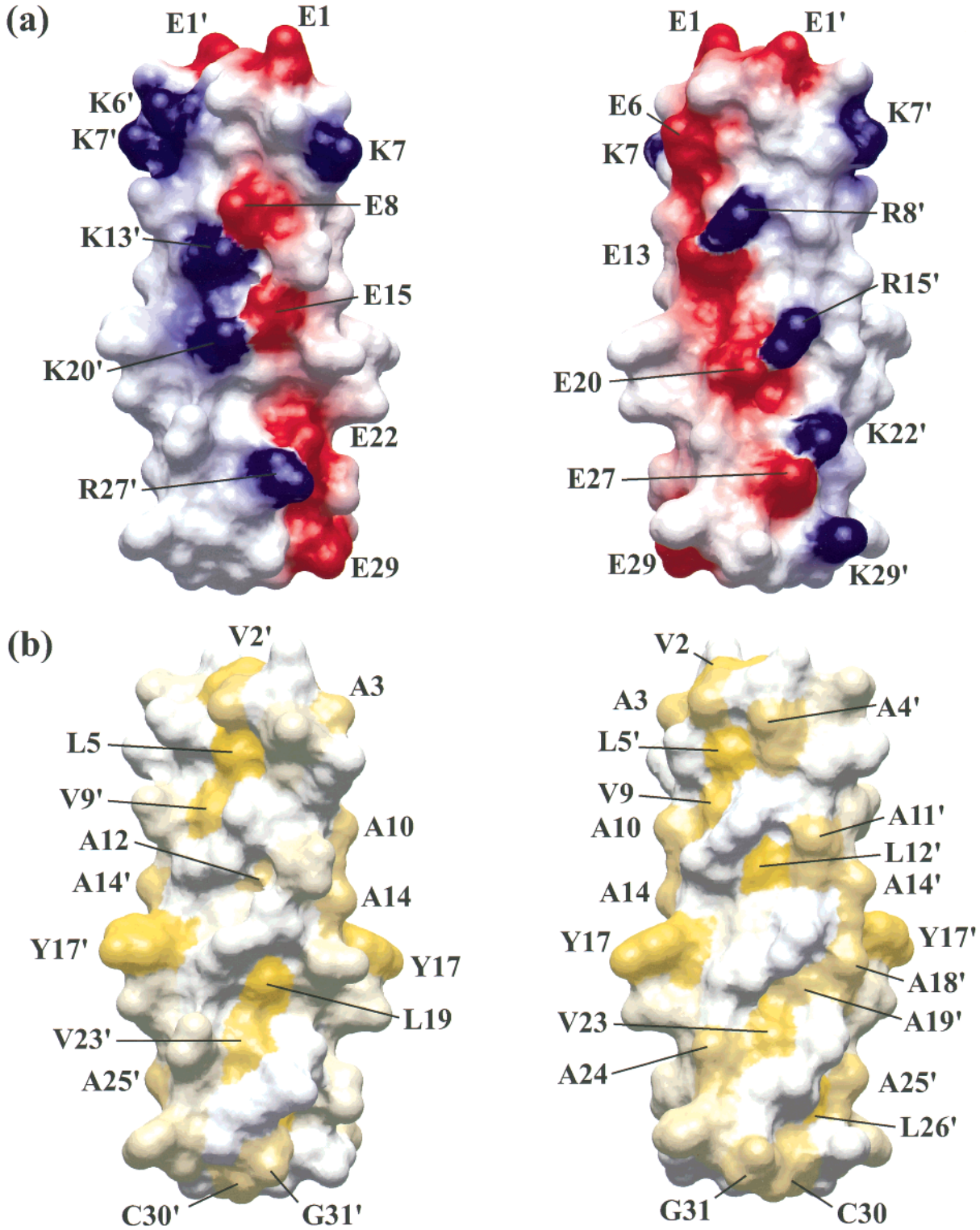

FIGURE 8: Contact surface of the minimized average structure of the AB zipper. (a) The surface is colored according to the electrostatic potential. Positive, neutral, and negative potentials are shown in blue, white, and red, respectively. The color intensity reflects the relative strength of the potentials (*64*). Front and back views of the zipper are depicted. (b) The hydrophobic areas on the zipper surface are colored in yellow. The intensity of the color is proportional to the hydrophobicity of the residues' side chains (*77*). The orientation of the molecules is the same as in panel a.

functional groups and hydrophobic packing of the side chains' methylene groups against the apolar helix interface.

Solvent Accessibility. The percentage of solvent accessible surface[6] on the side chains in the four heptad pairs of the AB zipper was calculated by reference to a linear, extended model peptide (Figure 7, panel b). As expected, residues in positions *a* and *d* forming the hydrophobic interface are the least accessible. Val$^{2,2'}$ in position *a* of the first heptad pair are more exposed (accessibilities of 46.9 and 37.7%,

[6] 21.9 ± 12.5% (16.8 ± 10.5%), 81.8 ± 1.6% (81.5 ± 2.5%), 72.6 ± 4.1% (68.6 ± 7.4%), 7.8 ± 5.2% (7.6 ± 2.5%), 54.6 ± 4.5% (53.6 ± 5.0%), 76.7 ± 7.0% (78.3 ± 9.6%), and 47.8 ± 10.3% (61.9 ± 7.4%) resulted for residues in positions *a* to *g* of the acidic (basic) helix.

respectively) due to their closeness to the N-terminal ends. Side chains of residues in *e* and *g* positions are exposed by 47.8 to 61.9%. Their alignment across the chain interface helps to shield interface residues *a* and *d* from solvent.

Determination of pK_a Values of Glu δ-Carboxylate Groups. The chemical shift of Glu H$^\gamma$ resonances depends on the protonation state of the side chains' carboxylate group (*78*) and can be used to determine pK_a values. The chemical shift change of Glu H$^\gamma$ has been followed in 2D TOCSY experiments recorded between pH 7 and 1.5 at very low ionic strength where variation of pK_a's are more pronounced because of lack of salt screening. Cross-peaks connecting H^N to H$^{\gamma 2,\gamma 3}$ provided unique H$^\gamma$ chemical shifts since only minor peak overlap occurred within the investigated pH range. All Glu H$^\gamma$ showed sufficiently large chemical shift changes to keep chemical shift reading errors low (Figure 9). Fitting of the experimental data to eq 4 was performed with either a constant Hill coefficient of $n = 1$ or with n as a free parameter (Table 4). In general, pK_a's thus fitted are comparable. The largest difference in pK_a (0.09 units) is observed for Glu^6 H$^{\gamma'}$ for which n is 0.75. For the remaining Glu H$^\gamma$ resonances, the fitted n varied between 0.84 ± 0.07. n smaller than 1 implies negative cooperativity, which may be caused by nearby groups titrating with a similar ionization constant; $n \leq 1$ is seen frequently in NMR pH titration experiments (*37*, *52*, *79*).

Glu$^{1,1'}$ in the less structured N-terminal tails have pK_a values of 4.14 ± 0.02 and 4.22 ± 0.02, respectively. These pK_a's closely resemble those of Glu located in short model peptides at 35 °C (*80*), in unfolded peptide segments of GCN4 at 25 °C (*36*) or in the N-terminal tail of matrilin-1 at 50 °C (*37*), the latter two measured at an ionic strength of 0.15 M. In comparison, the pK_a of AcGluOMe is between 4.3 and 4.4 (*36*, *37*, *81*). In case of the Glu's located within the coiled coil proper of the AB zipper, plotting of the pK_a versus the sequence number results in a V-shaped curve (Figure 10, panel a). In comparison with model compound Glu, residues positioned close to the ends of the structured coiled coil, in particular Glu^6 and Glu^{22}, have relatively high pK_a's (~4.82). Glu residues in the Glu^8−Glu^{20} peptide segment reveal moderately shifted pK_a's (~4.11−4.52), Glu^{15}, located in the center of the sequence, having the lowest pK_a (~4.11).

Sigmoidal pH dependence of the chemical shift, suggesting vicinity to a titratable group, is observed for 19 H^N resonances of the acidic chain. Plotting of the pK_a versus the sequence number results in a curve that follows a similar trend as seen for the pK_a obtained from Glu H$^\gamma$ chemical shift data (Figure 10, panel a). It appears therefore that the chemical shift of backbone H^N is largely affected by the ionization state of Glu close in sequence. 12 H^N resonances of the basic helix shift sigmoidally with respect to pH, and the fitted pK_a reflect the ionization behavior of Glu located nearby (data not shown). The total chemical shift change $\Delta\delta$ of backbone H^N, on going from pH 7.0 to pH 1.5 is illustrated in Figure 10, panels b and c. In case of the acidic helix, many Glu residues and some of their immediate neighbors display negative $\Delta\delta$(H^N). Hence, closeness of these H^N to Glu C$^\delta$OO$^-$ is likely. The low-field shift at neutral pH is due to deshielding of H^N upon interaction with the charged Glu carboxylate group. In the basic helix, low-field shifts upon raising of the pH are observed for residues opposing Glu on the juxtaposed chain. In general, $|\Delta\delta(H^N)|$ is smaller than 0.15 ppm indicative of only weak interaction with the corresponding Glu side chains. The largest negative $\Delta\delta$(H^N) is observed for Gln$^{3'}$, which is involved in partial H-bonding with the δ-carboxylate group of Glu$^{1'}$ in the calculated structures.

Contribution of Charged Glu to Stability of the Coiled Coil. The difference in the pK_a of an ionizable residue measured in the folded and unfolded protein reflects the difference in the contribution to protein stability of the residue in charged and uncharged form, respectively (*32*, *35*, *36*). The influence of the protonation state of a particular Glu residue on the free energy of folding is defined as

$$\Delta\Delta G_F = \Delta G_{F,-} - \Delta G_{F,0} \quad (5)$$

where $\Delta G_{F,-}$ refers to the charged form and $\Delta G_{F,0}$ refers to the uncharged form of the residue. $\Delta\Delta G_F$ can be expressed as

$$\Delta\Delta G_F = -2.303RT(\mathrm{p}K_a^U - \mathrm{p}K_a^F) \quad (6)$$

where superscripts U and F refer to the unfolded and folded protein, respectively. If $pK_a^F > pK_a^U$, $\Delta\Delta G_F$ is positive: the protonated, uncharged form of the acidic group is more stabilizing. If $pK_a^F < pK_a^U$, $\Delta\Delta G_F$ is negative: the deprotonated, charged form of the acidic group is more stabilizing. Hence, if a charged residue is contributing favorably to ΔG_F by forming a stable salt bridge, one expects a lower pK_a in the folded than in the unfolded protein. To calculate $\Delta\Delta G_F$, one has to know the pK_a values in the unfolded protein, which may be deduced from protein fragments containing the acidic residues of interest. However, protein fragments are not a complete representation of the denatured state and both local and nonlocal sequence effects may perturb the pK_a's. Also, pK_a's of the unfolded state when deduced from protein fragments often vary depending on the chosen size of the fragments (*82*). As an alternative, the pK_a value of model compound AcGluOMe, which is 4.3−4.4 (*36*, *37*, *81*), may serve as reference. Because of desolvation effects and electrostatic interactions with other charged groups and permanent dipoles, the pK_a value decreases when placing the residue in an unstructured peptide chain (*35*): a pK_a value of 4.2 was identified for Glu located in the tetrapeptide G−G−E−A (*80*). Values of similar magnitude were obtained for Glu in unfolded peptide segments of coiled coils (*36*, *37*) or for Glu$^{1,1'}$ positioned at the less structured N-terminus of the AB zipper in this study. Assuming that the pK_a's in the unfolded protein equal 4.4 of model compound AcGluOMe, the sum of the $\Delta\Delta G_F$'s amounts to 0.98 kcal mol^{-1}. Assuming pK_a = 4.2 in the unfolded peptide, the sum of the $\Delta\Delta G_F$'s is 3.82 kcal mol^{-1}. Hence, independent of the reference pK_a applied, the net contribution of the charged Glu side chains is destabilizing. Heat denaturation experiments monitored by CD disclose a change of ΔG_F ($= -\Delta G_U$) of ~1.6 kcal mol^{-1} when increasing the pH from 4 to 8 (Table 1). This value is similar to the summed $\Delta\Delta G_F$'s assuming pK_a = 4.4 in the unfolded protein. The contribution of the 10 Glu residues to the net charge of the AB zipper is −10 and −2.7 at pH 8 and 4, respectively. A substantial decrease in ΔG_F is already observed when changing the pH from 8 to 6 (−0.5 kcal mol^{-1}, Table 1), even though the net

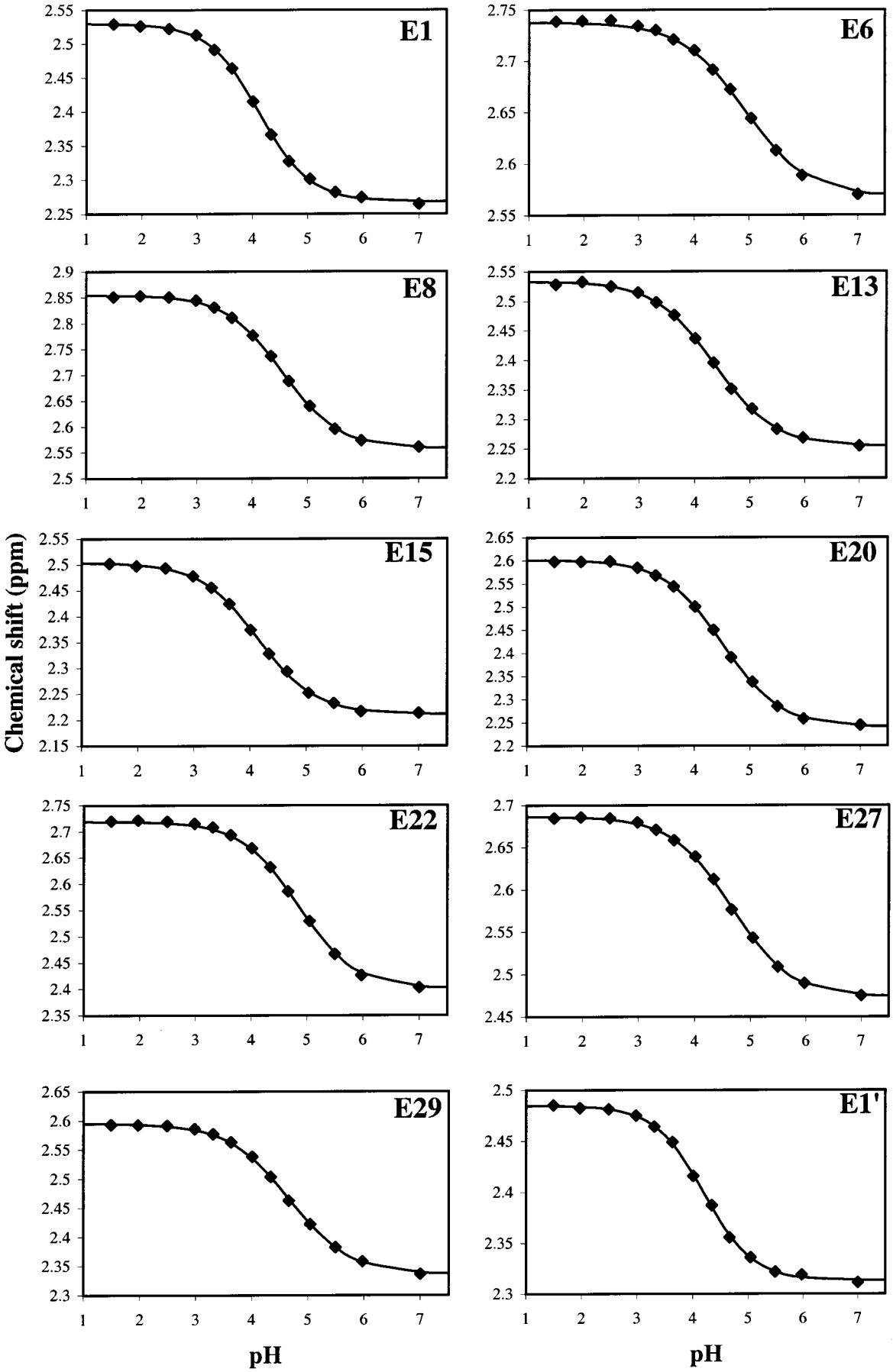

FIGURE 9: pH titration curves of Glu H$^{\gamma}$ resonances. Chemicals shifts extracted from 2D TOCSY experiments recorded at 37 °C are plotted versus the pH. The solid line was determined by nonlinear least-squares fitting of the experimental data (◆) to eq 4 applying the Hill-coefficient *n* as free parameter.

Table 4: ^{1}H NMR pH Titration of Glu H$^\gamma$ Resonances of the AB Zipper at 37 °C: Parameters pK_a, δ_a, δ_b, and n Derived by Nonlinear Least Squares Fitting of Chemical Shift Data to a Modified Form of the Henderson−Hasselbalch Equation (eq 4)

resonance		p$K_{a\ (n=1)}$[a]	p$K_{a\ (\text{fitted } n)}$[a]	δ_a (ppm)[b]	δ_b (ppm)[b]	n	average pK_a[c]
E^1	H$^\gamma$	4.12	4.12	2.53 (δ_1)[d]	2.27 (δ_1)	0.95	4.14 ± 0.02
	H$^{\gamma'}$	4.16	4.16	2.54 (δ_1)	2.34 (δ_1)	0.93	
E^6	H$^{\gamma'}$	4.75	4.81	2.74 (δ_1)	2.57 (δ_1)	0.73	4.82 ± 0.07
	H$^{\gamma'}$	4.82	4.91	2.74 (δ_2)	2.57 (δ_2)	0.75	
E^8	H$^\gamma$	4.51	4.53	2.52 (δ_2)	2.27 (δ_2)	0.85	4.52 ± 0.01
	H$^{\gamma'}$	4.52	4.54	2.85 (δ_1)	2.56 (δ_1)	0.85	
	H$^{\gamma'}$	4.51	4.53	2.85 (δ_2)	2.56 (δ_2)	0.85	
E^{13}	H$^\gamma$	4.33	4.35	2.53 (δ_2)	2.25 (δ_2)	0.80	4.37 ± 0.03
	H$^{\gamma'}$	4.38	4.43	2.72 (δ_1)	2.54 (δ_1)	0.69	
	H$^{\gamma'}$	4.37	4.38	2.72 (δ_2)	2.55 (δ_2)	0.82	
E^{15}	H$^\gamma$	4.13	4.14	2.50 (δ_1)	2.21 (δ_1)	0.84	4.11 ± 0.02
	H$^\gamma$	4.09	4.09	2.50 (δ_2)	2.22 (δ_2)	0.90	
	H$^{\gamma'}$	4.09	4.09	2.58 (δ_1)	2.43 (δ_1)	0.96	
E^{20}	H$^\gamma$	4.44	4.46	2.62 (δ_1)	2.25 (δ_1)	0.87	4.41 ± 0.07
	H$^\gamma$	4.48	4.50	2.60 (δ_2)	2.24 (δ_2)	0.83	
	H$^{\gamma'}$	4.36	4.37	2.62 (δ_1)	2.48 (δ_1)	0.82	
	H$^{\gamma'}$	4.33	4.35	2.63 (δ_2)	2.48 (δ_2)	0.79	
E^{22}	H$^\gamma$	4.82	4.88	2.45 (δ_2)	2.21 (δ_2)	0.82	4.82 ± 0.03
	H$^{\gamma'}$	4.79	4.83	2.72 (δ_1)	2.40 (δ_1)	0.84	
	H$^{\gamma'}$	4.79	4.83	2.72 (δ_2)	2.40 (δ_2)	0.85	
E^{27}	H$^{\gamma*}$	4.65	4.70	2.68 (δ_1)	2.47 (δ_1)	0.82	4.65 ± 0.04
	H$^{\gamma*}$	4.61	4.65	2.69 (δ_2)	2.47 (δ_2)	0.81	
E^{29}	H$^\gamma$	4.62	4.67	2.60 (δ_1)	2.34 (δ_1)	0.79	4.63 ± 0.03
	H$^\gamma$	4.62	4.67	2.59 (δ_2)	2.34 (δ_2)	0.80	
	H$^{\gamma'}$	4.61	4.62	2.69 (δ_1)	2.45 (δ_1)	0.91	
	H$^{\gamma'}$	4.60	4.61	2.70 (δ_2)	2.45 (δ_2)	0.91	
E$^{1'}$	H$^\gamma$	4.20	4.20	2.48 (δ_1)	2.31 (δ_1)	0.99	4.22 ± 0.02
	H$^{\gamma'}$	4.22	4.24	2.56 (δ_1)	2.37 (δ_1)	0.84	

[a] pK_a values obtained by fitting experimental data to eq 4 using constant ($n = 1$) and variable Hill coefficient, respectively. [b] Upper and lower chemical shift limits fitted with n as free evolving parameter. [c] Average of pK_a values derived by fitting with constant as well as variable n. [d] δ_1 and δ_2 denote dimensions along t_1 and t_2, respectively.

charge contribution of Glu at pH 6 is still −9.7. This observation points at additional factors, besides the charge of Glu, affecting the stability of the coiled coil such as the dependence of the helical propensity and hydrophobicity of residues on pH.

To summarize, pK_a data suggest that the majority of the charged Glu residues of the AB zipper contribute unfavorably to the stability of the coiled coil. In particular, Glu's in positions 6, 8, 22, 27, and 29 display significantly upward shifted pK_a's and seem to be a source for the lower stability of the zipper at neutral pH. Charged Glu's located at the N-terminus and near the center of the peptide play only a marginal role in stabilizing or destabilizing the protein as indicated by their pK_a values being similar to reference values for Glu's in unfolded peptides. In case of Glu$^{1,1'}$, higher pK_a values might be expected due to mutual charge repulsion. However, Glu's near the N-terminus of the helix "feel" the helix dipole, which may lower the pK_a.

In general, results are in line with studies on the contribution of Glu^{20} and Glu^{22} to the stability of GCN4 (*36*), both residues being involved in salt bridges with Lys$^{15'}$ and Lys$^{27'}$, respectively, in the X-ray structure (*8*). pK_a values of 4.44 and 4.13 have been determined for the folded form suggesting unfavorable and negligible contribution of the charged Glu to stability. Interestingly, Glu^{20} in both GCN4 and the AB zipper display very similar protonation constants (4.44 and 4.41, respectively) indicative of being slightly destabilizing in charged form. In contrast to Glu^{22} in GCN4, the corresponding residue of the AB zipper has a higher pK_a (4.82). Glu^{22} of GCN4 is able to form ion pairs with Lys$^{27'}$ and Arg^{25}, the latter located on the same helix, whereas Glu^{22} of the AB zipper has no opportunity for intrahelical ion pairing. pK_a values of the AB zipper are also comparable to the pK_a's of the eight Glu residues in homotrimeric matrilin-1: a destabilizing role was reported for two of the Glu's, while only marginal effects on the stability were encountered for the remaining Glu's (*37*).

In all the studies on pK_a values of Glu in coiled coils published thus far, including the present work, the contribution of charged Glu to stability is either unfavorable, negligible, or at best slightly favorable. The question of whether electrostatic interhelix interactions do occur at all in coiled coils remains to be discussed now. NOE connectivities of the AB zipper reveal a distinct pattern of interresidue contacts involving *g* and *e* position residues (Table 3). Such contacts, in particular those with *a′* and *d′* position residues of the juxtaposed helix emphasize the relatively defined spatial alignment of these side chains. As shown in Figure 6, panel a, the conformation of side chains is flexible. Yet each ensemble of side chains points into the same specific direction leading to partial electrostatic interactions between *g* and *e′*(+1) position residues as well as hydrophobic interactions with the chain interface. In a study about stability of engineered salt bridges in T4 lysozyme, it was concluded that ionic interactions among charged residues located on the protein surface are not favorable since the electrostatic energy term is outweighed by a large unfavorable entropic term for fixing the residues in a specific conformation (*83*). In the AB zipper, the charged side chains show some conformational variability (Figure 6, panel a), which may keep unfavorable entropic contribution low. The fact of the zipper being more stable at acidic pH suggests

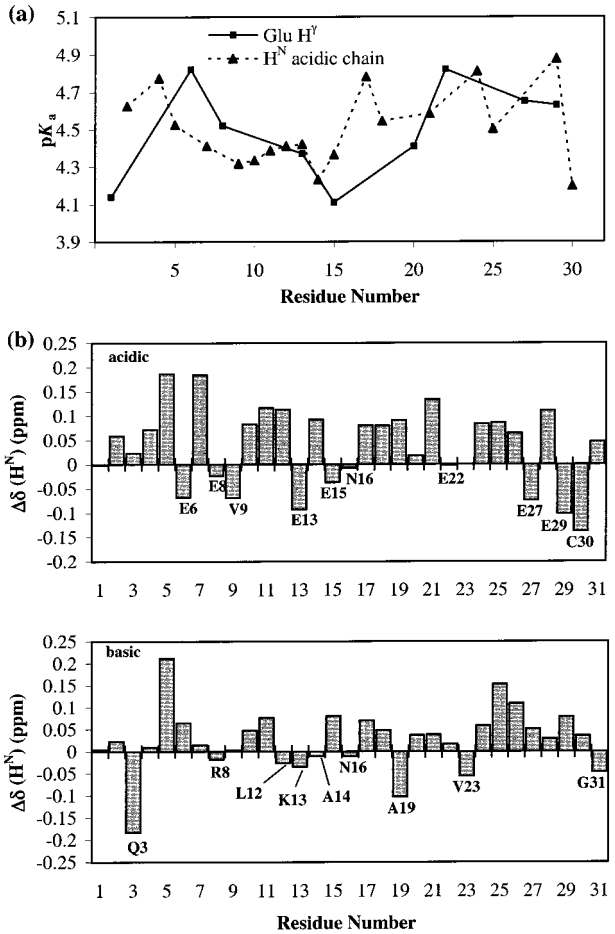

FIGURE 10: Summary of pK_a values derived from the pH dependence of chemical shifts of Glu H^{γ} and H^N and overview of total chemical shift changes $\Delta\delta$ of backbone H^N. (a) pK_a values determined by nonlinear least-squares fitting (eq 4) of chemical shift data on Glu H^{γ} (■, solid line) and H^N (▲, dashed line) of the acidic helix are plotted versus the sequence number. (b) The total chemical shift changes $\Delta\delta$ of H^N resonances in the acidic (top panel) and basic (bottom panel) helix of the zipper are represented by bar diagrams. Positive and negative amplitudes of the bars indicate low- and high-field shifts of the resonances upon lowering the pH value from 7.0 to 1.5. Residues showing high-field shifted H^N resonances at low pH are explicitly denoted.

that the driving force for the alignment of the residues is of hydrophobic rather than of electrostatic nature. Higher stability at low pH has also been reported by Zhou et al. (*27*, *33*) for a designed homodimeric coiled coil with 10 potential $g/e'(+1)$ ion pairs. Double mutant cycle analysis yielded contributions to stability of -0.37 kcal mol^{-1} for the interhelical ion pairs involving charged Glu, and of -0.65 kcal mol^{-1} for the protonated form of Glu. Hence, although the energetic term of the ionic interaction may seem favorable at neutral pH, it is offset by an even more favorable energetic term gained from a uncharged Glu at low pH. Uncharged Glu is characterized by higher helical preference as well as higher hydrophobicity allowing a better packing of the side chain against apolar residues located at the chain interface (*22*).

In the NMR structures of the AB zipper, Glu^{22} in particular seems to form an interhelical salt bridge with $Arg^{27'}$ yet this Glu displays a high pK_a value. This, however, is no contradiction since $\Delta\Delta G_F$, though apparently unfavorable, does not reveal single energy terms, such as the electrostatic, hydrophobic, or entropic contributions to stability. In addition, the pK_a value is affected by electrostatic interactions with other charged groups in the molecule. Hence, the favorable energy of the $Glu^{22}-Arg^{27'}$ interaction might be outweighed by unfavorable electrostatic interactions with other negatively charged groups shifting the pK_a upward. Indeed, electrostatic calculations (*63*, *84*, *85*) on the minimized average structure of the AB zipper predict high pK_a's for Glu^6 and Glu^{22} despite an ionic bond of the latter to $Arg^{27'}$. Likewise, favorable hydrophobic interactions of an uncharged Glu might increase its pK_a. With the aim at decomposition of ΔG_F into the individual energetic terms, we are presently performing extensive calorimetric experiments on the AB zipper as well as continuum electrostatic calculations based on the NMR solution structures presented here.

ACKNOWLEDGMENT

We thank Frank Löhr for the acquisition of 800 MHz NMR data at the large-scale NMR facility of the Johann Wolfgang Goethe University in Frankfurt, Germany, Martin Binder for expert help with the NMR spectrometer, Alemayehu Abebe for stimulating discussion about electrostatic calculations, Stefan Klauser for the peptide synthesis, and Peter Gehrig for mass spectrometry of the peptides.

SUPPORTING INFORMATION AVAILABLE

Table of ^{1}H NMR chemical shifts of the AB zipper at pH* 5.65, 37 °C. This material is available free of charge via the Internet at http://pubs.acs.org.

REFERENCES

1. Crick, F. H. C. (1953) *Acta Crystallogr. 6*, 689−697.
2. Landschulz, W. H., Johnson, P. F., and McKnight, S. L. (1988) *Science 240*, 1759−1764.
3. Lupas, A. (1996) *Trends Biochem. Sci. 21*, 375−382.
4. Ellenberger, T. E., Brandl, C. J., Struhl, K., and Harrison, S. C. (1992) *Cell 71*, 1223−1237.
5. Glover, J. N. M., and Harrison, S. C. (1995) *Nature 373*, 257−261.
6. Hurst, H. C. (1995) *Protein Profile 2*, 101−168.
7. Oas, T. G., McIntosh, L. P., O'Shea, E. K., Dahlquist, F. W., and Kim, P. S. (1990) *Biochemistry 29*, 2891−2894.
8. O'Shea, E. K., Klemm, J. D., Kim, P. S., and Alber, T. (1991) *Science 254*, 539−544.
9. Saudek, V., Pastore, A., Morelli, M. A., Frank, R., Gausepohl, H., and Gibson, T. (1991) *Protein Eng. 4*, 519−529.
10. Junius, F. K., O'Donoghue, S. I., Nilges, M., Weiss, A. S., and King, G. F. (1996) *J. Biol. Chem. 271*, 13663−13667.
11. Junius, F. K., Weiss, A. S., and King, G. F. (1993) *Eur. J. Biochem. 214*, 415−424.
12. Lavigne, P., Crump, M. P., Gagné, S. M., Hodges, R. S., Kay, C. M., and Sykes, B. D. (1998) *J. Mol. Biol. 281*, 165−181.
13. Whitby, F. G., Kent, H., Stewart, F., Stewart, M., Xie, X., Hatch, V., Cohen, C., and Phillips, G. N., Jr. (1992) *J. Mol. Biol. 227*, 441−452.
14. Greenfield, N. J., Montelione, G. T., Farid, R. S., and Hitchcock-DeGregori, S. E. (1998) *Biochemistry 37*, 7834−7843.
15. Dames, S. A., Kammerer, R. A., Wiltscheck, R., Engel, J., and Alexandrescu, A. T. (1998) *Nat. Struct. Biol. 5*, 687−691.
16. Junius, F. K., Mackay, J. P., Bubb, W. A., Jensen, S. A., Weiss, A. S., and King, G. F. (1995) *Biochemistry 34*, 6164−6174.
17. Harbury, P. B., Zhang, T., Kim, P. S., and Alber, T. (1993) *Science 262*, 1401−1407.
18. Wendt, H., Berger, C., Baici, A., Thomas, R. M., and Bosshard, H. R. (1995) *Biochemistry 34*, 4097−4107.

19. Jelesarov, I., and Bosshard, H. R. (1996) *J. Mol. Biol. 263*, 344−358.
20. Wendt, H., Leder, L., Härmä, H., Jelesarov, I., Baici, A., and Bosshard, H. R. (1997) *Biochemistry 36*, 204−213.
21. Jelesarov, I., Dürr, E., Thomas, R. M., and Bosshard, H. R. (1998) *Biochemistry 37*, 7539−7550.
22. Dürr, E., Jelesarov, I., and Bosshard, H. R. (1999) *Biochemistry 38*, 870−880.
23. Lumb, K. J., and Kim, P. S. (1995) *Biochemistry 34*, 8642−8648.
24. Gonzalez, L., Jr., Woolfson, D. N., and Alber, T. (1996) *Nat. Struct. Biol. 3*, 1011−1018.
25. O'Shea, E. K., Rutkowski, R., Stafford, W. F., III, and Kim, P. S. (1989) *Science 245*, 646−648.
26. O'Shea, E. K., Lumb, K. J., and Kim, P. S. (1993) *Curr. Biol. 3*, 658−667.
27. Zhou, N. E., Kay, C. M., and Hodges, R. S. (1994) *J. Mol. Biol. 237*, 500−512.
28. Kohn, W. D., Kay, C. M., and Hodges, R. S. (1995) *Protein Sci. 4*, 237−250.
29. Spek, E. J., Bui, A. H., Lu, M., and Kallenbach, N. R. (1998) *Protein Sci. 7*, 2431−2437.
30. Hendsch, Z. S., and Tidor, B. (1999) *Protein Sci. 8*, 1381−1392.
31. Lavigne, P., Sönnichsen, F. D., Kay, C. M., and Hodges, R. S. (1996) *Science 271*, 1136−1137.
32. Lumb, K. J., and Kim, P. S. (1996) *Science 271*, 1137−1138.
33. Zhou, N. E., Kay, C. M., and Hodges, R. S. (1994) *Protein Eng. 7*, 1365−1372.
34. Krylov, D., Mikhailenko, I., and Vinson, C. (1994) *EMBO J. 13*, 2849−2861.
35. Yang, A.-S., and Honig, B. (1992) *Curr. Opin. Struct. Biol. 2*, 40−45.
36. Lumb, K. J., and Kim, P. S. (1995) *Science 268*, 436−439.
37. Dames, S. A., Kammerer, R. A., Moskau, D., Engel, J., and Alexandrescu, A. T. (1999) *FEBS Lett. 446*, 75−80.
38. Rink, H. (1987) *Tetrahedron Lett. 28*, 3787−3790.
39. Shortle, D., Meeker, A. K., and Freire, E. (1988) *Biochemistry 27*, 4761−4768.
40. Makhatadze, G. I., and Primalov, P. L. (1995) *Adv. Protein Chem. 47*, 307−425.
41. Piantini, U., Sørensen, O. W., and Ernst, R. R. (1982) *J. Am. Chem. Soc. 104*, 6800−6801.
42. States, D. J., Haberkorn, R. A., and Ruben, D. J. (1982) *J. Magn. Reson. 48*, 286−292.
43. Bax, A., and Davis, D. G. (1985) *J. Magn. Reson. 65*, 355−360.
44. Shaka, A. J., Lee, C. J., and Pines, A. (1988) *J. Magn. Reson. 77*, 274−293.
45. Briand, J., and Ernst, R. R. (1991) *Chem. Phys. Lett. 185*, 276−285.
46. Piotto, M., Saudek, V., and Sklenár, V. (1992) *J. Biomol. NMR 2*, 661−665.
47. Sklenár, V., Piotto, M., Leppik, R., and Saudek, V. (1993) *J. Magn. Reson. Ser. A 102*, 241−245.
48. Marti, D. N., Hu, C.-K., An, S. S. A., von Haller, P., Schaller, J., and Llinás, M. (1997) *Biochemistry 36*, 11591−11604.
49. Friedrichs, M. S. (1995) *J. Biomol. NMR 5*, 147−153.
50. De Marco, A. (1977) *J. Magn. Reson. 26*, 527−528.
51. Edsall, J. T., and Wymann, J. (1958) *Biophysical Chemistry*, Chapter 8, Academic Press, New York.
52. Markley, J. L. (1975) *Acc. Chem. Res. 8*, 70−80.
53. Wüthrich, K., Billeter, M., and Braun, W. (1983) *J. Mol. Biol. 169*, 949−961.
54. De Marco, A., Llinás, M., and Wüthrich, K. (1978) *Biopolymers 17*, 617−636.
55. Pardi, A., Billeter, M., and Wüthrich, K. (1984) *J. Mol. Biol. 180*, 741−751.
56. Nilges, M., Kuszewski, J., and Brünger, A. T. (1991) in *Computational Aspects of the Study of Biological Macromolecules by NMR* (Hoch, J. C., Ed.) Plenum Press, New York.
57. Kuszewski, J., Nilges, M., and Brünger, A. T. (1992), *J. Biomol. NMR 2*, 33−56.
58. Marti, D. N., Schaller, J., and Llinás, M. (1999) *Biochemistry 38*, 15741−15755.
59. Brünger, A. T. (1992) *X-PLOR 3.1 User Manual*, Yale University Press, New Haven, CT.
60. Linge, J. P., and Nilges, M. (1999) *J. Biomol. NMR 13*, 51−59.
61. Jorgensen, W. L., Chandrasekhar, J., Madura, J. D., Impey, R. W., and Klein, M. L. (1983) *J. Chem. Phys. 79*, 926−935.
62. Laskowsky, R. A., MacArthur, M. W., Moss, D. S., and Thornton, J. M. (1993) *J. Appl. Crystallogr. 26*, 283−291.
63. Vriend, G. (1990) *J. Mol. Graphics 8*, 52−56.
64. Koradi, R., Billeter, M., and Wüthrich, K. (1996) *J. Mol. Graphics 14*, 51−55.
65. Mach, H., Middaugh, C. R., and Lewis, R. V. (1992) *Anal. Biochem. 200*, 74−80.
66. Chen, Y.-H., Yang, J. T., and Chau, K. H. (1974) *Biochemistry 13*, 3350−3359.
67. Zhou, N. E., Kay, C. M., and Hodges, R. S. (1992) *Biochemistry 31*, 5739−5746.
68. Wishart, D. S., Sykes, B. D., and Richards, F. M. (1991) *J. Mol. Biol. 222*, 311−333.
69. Wüthrich, K. (1986) *NMR of Proteins and Nucleic Acids*, John Wiley and Sons, New York.
70. Markley, J. L., Bax, A., Arata, Y., Hilbers, C. W., Kaptein, R., Sykes, B. D., Wright, P. E., and Wüthrich, K. (1998) *Eur. J. Biochem. 256*, 1−15.
71. Ramachandran, G. N., and Sasisekharan, V. (1968) *Adv. Protein Chem. 23*, 283−438.
72. Jorgensen, W. L., and Tirado-Rives, J. (1988) *J. Am. Chem. Soc. 110*, 1657−1666.
73. Goodman, E. M., and Kim, P. S. (1991) *Biochemistry 30*, 11615−11620.
74. Pardi, A., Wagner, G., and Wüthrich, K. (1983) *Eur. J. Biochem. 137*, 445−454.
75. Mackay, J. P., Shaw, G. L., and King, G. F. (1996) *Biochemistry 35*, 4867−4877.
76. Lavigne, P., Kondejewski, L. H., Houston, M. E., Jr., Sönnichsen, F. D., Lix, B., Sykes, B. D., Hodges, R. S., and Kay, C. M. (1995) *J. Mol. Biol. 254*, 505−520.
77. Roseman, M. A. (1988) *J. Mol. Biol. 200*, 513−522.
78. Szyperski, T., Antuch, W., Schick, M., Betz, A., Stone, S. R., and Wüthrich, K. (1994) *Biochemistry 33*, 9303−9310.
79. Tan, Y.-J., Oliveberg, M., and Fersht, A. R. (1995) *J. Mol. Biol. 254*, 980−992.
80. Richarz, R., and Wüthrich, K. (1978) *Biopolymers 17*, 2133−2141.
81. Nozaki, Y., and Tanford, C. (1967) *Methods Enzymol. 11*, 715−734.
82. Kuhlman, B., Luisi, D. L., Young, P., and Raleigh, D. P. (1999) *Biochemistry 38*, 4896−4903.
83. Dao-pin, S., Sauer, U., Nicholson, H., and Matthews, B. W. (1991) *Biochemistry 30*, 7142−7153.
84. Nicholls, A., and Honig, B. (1991) *J. Comput. Chem. 12*, 435−445.
85. Nielsen, J. E., Andersen, K. V., Honig, B., Hooft, R. W. W., Klebe, G., Vriend, G., and Wade, R. C. (1999) *Protein Eng. 12*, 657−662.

BI001242E